

CHAPTER 40

Behavior of Plasma-Sprayed Coatings

CHRISTOPHER C. BERNDT

INTRODUCTION

Plasma-spray techniques are well-established as a means of depositing corrosion, wear resistant, and thermal barrier coatings. Previous publications have discussed coating properties in relation to plasma-spray **variables**,⁽¹⁾ by thermofluid and heat transfer **models**^(2,3,4) and by examining the microstructure.⁽⁵⁾ Several **books**^(6,7) and conference **proceedings**^(8,9,10,11) have also addressed the general field of thermal spraying technology.

This chapter describes the microstructural development of plasma-sprayed oxide coatings and relates microstructural details to their mechanical behavior. Specific examples are drawn from experience with aluminum oxide coatings and thermal **barrier** coatings of yttria stabilized zirconia.

MICROSTRUCTURAL OBSERVATIONS

Optical Metallography

Routine metallography was used to investigate the morphology of plasma-sprayed materials. The splat nature of particles is well-characterized and the lamellar structure formed during deposition is used during quality assurance to check for coating integrity and as a measure of particle melting, inclusions, and porosity. Figure 40.1 shows a single splat of alumina that was sprayed onto a machine-ground steel substrate. The main features to note are that (1) the ceramic splat has spread out significantly over the substrate,



Figure 40.1 Plasma-spray quenched particle of Al_2O_3 .

(2) the splat in some areas is transparent (region A) to electrons and is therefore very thin, and (3) microcracks and various forms of porosity (interfacial about B and near the splat surface in C) can be distinguished.

Metallic powders are usually deposited under different plasma-spray variables because of their lower melting point. The thermal and velocity properties at the moment of impact with the substrate are different from oxides and this is reflected in their microstructure. These particles reveal complete melting and no obvious signs of gross porosity or microcracks.

These two different structures are often used in conjunction. For example, a primary coating of the composite powder Ni-Al adheres well to a grit-blast substrate and in turn provides an excellent surface for a ceramic overlay. This "laminar" composite shows very interesting mechanical properties, as illustrated in another section.

Scanning Electron Microscopy and Transmission Electron Microscopy

Figure 40.2 shows a coating cross section (i.e., perpendicular to the substrate). The individual "saucer-shaped" particles can be discerned and some splats (area A) exhibit columnar grains growing perpendicular to the substrate. Such observations, together with fundamental TEM work,^(5,12) confirm models of material and heat flow during rapid solidification. Thus, for the ideal case of intimate contact between a particle and substrate, there is grain growth perpendicular to the substrate surface. However, any part of

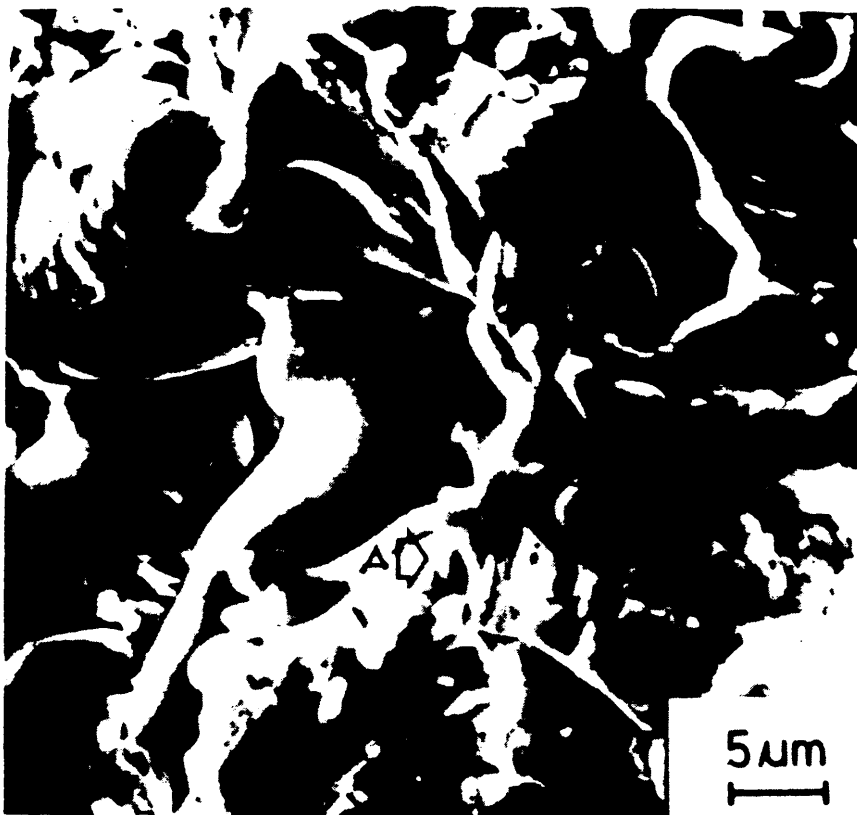


Figure 40.2 SEM of plasma-sprayed Al₂O₃ coating (Cross section).

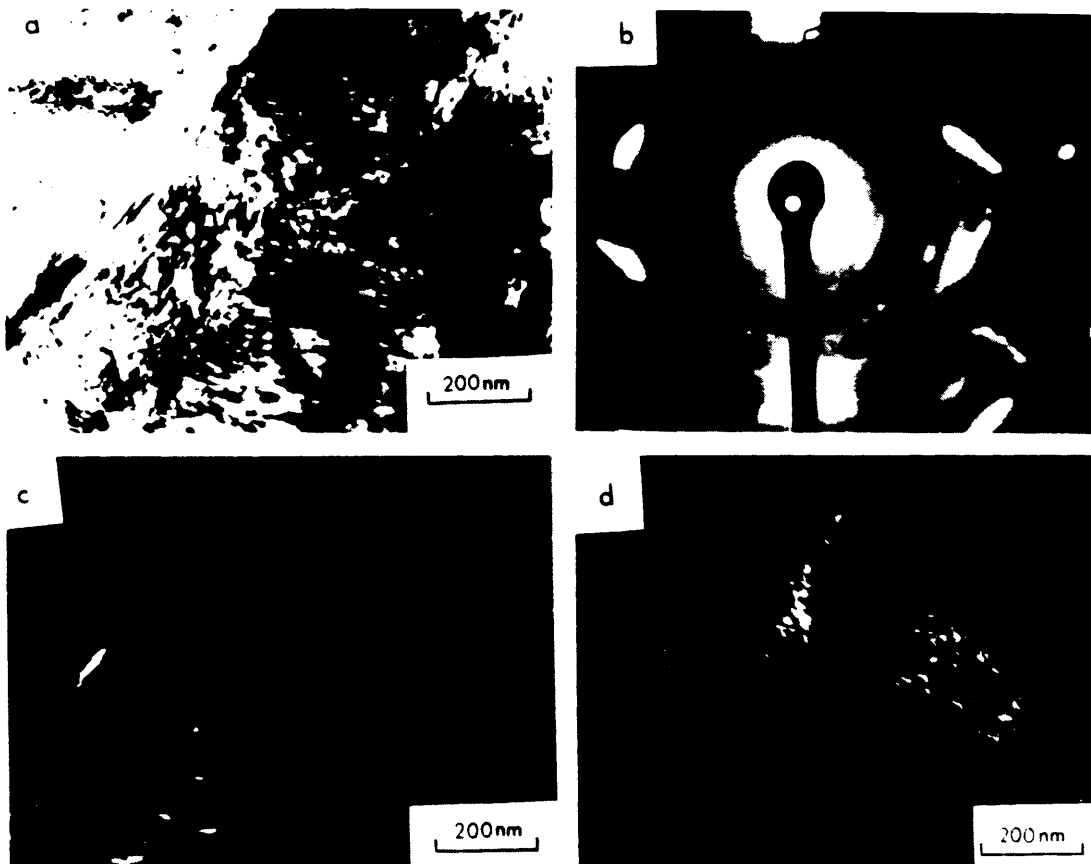


Figure 40.3 TEM of 8 wt. % Y₂O₃-ZrO₂ plasma-sprayed coating: (a) bright field, (b) diffraction pattern, (c) dark field of spot 1, and (d) dark field of spot 2.



Figure 40.4 TEM of 8 wt. % $\text{Y}_2\text{O}_3\text{-ZrO}_2$ plasma-sprayed coating.

the solidifying particle that peels from the substrate will show grain growth oriented in the longitudinal direction.

Further evidence of orientation effects can be observed via TEM. For example, the bright field image of an 8 wt. % yttria stabilized zirconia (YSZ) coating (Fig. 40.3a) revealed a grain structure with oriented microcrystals (Fig. 40.3b,c,d). However, other regions (Fig. 40.4) reveal an amorphous diffraction pattern for an area that exhibits very fine dendrites. The dendritic arm spacing can be used⁽¹³⁾ to calculate a cooling rate of 1.4×10^7 °C/sec, which correlates well with cooling rates obtained for other splat cooling processes.

FRACTURE PROPERTIES

Tensile Tests

The adhesion of the coating to the substrate is of paramount importance. The most common technique follows ASTM C633-69, where a fixture is glued directly on to the coating so that tensile loading conditions can be simulated. Other experimental methods⁽¹⁴⁾ based on the principles of fracture mechanics may be used for examining the mechanisms of failure. For example, Fig.

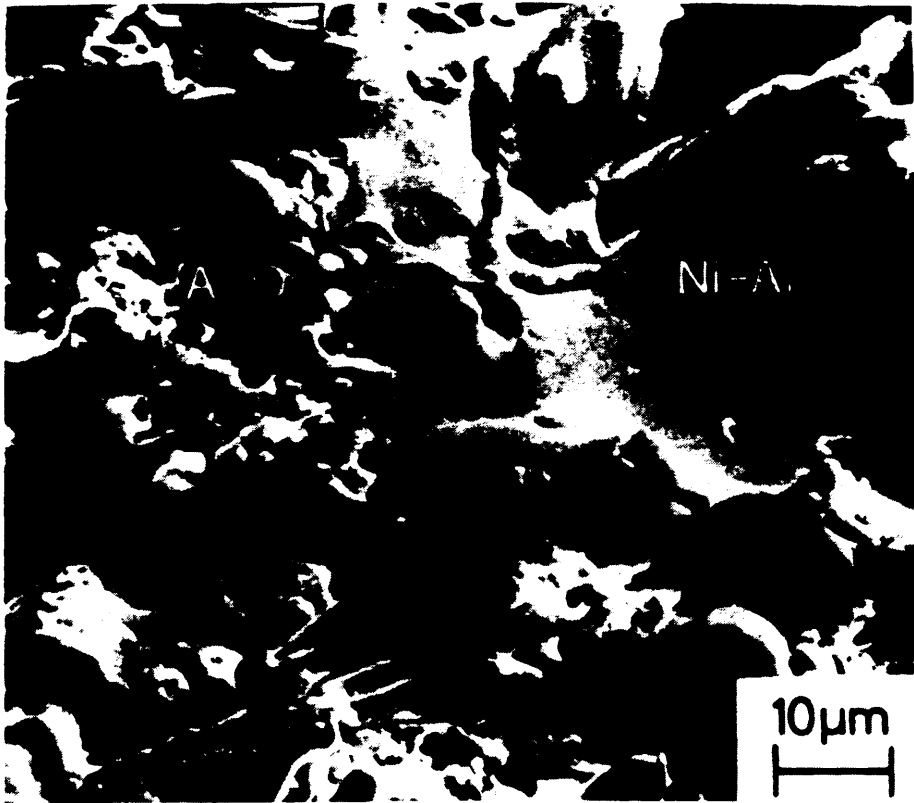


Figure 40.5 Failure through the bond coat-ceramic coat interfacial region of a fracture toughness specimen.

40.5 shows failure in the interfacial region of an alumina and bond coat (Ni–Al) system. The fracture toughness of this mixed mode failure was 58 J/m^{-2} , which contrasts with 21 and 319 J/m^{-2} for failure within the ceramic and bond coats, respectively.

Therefore, the fracture toughness tests have the distinct advantage of examining specific failure modes and correlating fundamental materials properties to the behavior of the bulk coating. Cracking in the interfacial region (Fig. 40.5) occurred by plastic deformation of the metallic particles and brittle fracture through the ceramic regions. It is also evident that the durability of the ceramic coating would be severely limited if no bond coat was incorporated. In fact, the weakest link in such a system would be the boundary at the substrate surface (12 J/m^{-2}), which can be compared with that of failure in the metal-ceramic system (21 J/m^{-2}). Thus, the incorporation of a bond coat also directs the failure mode away from the interfacial region to within the ceramic. It was noted (Fig. 40.1) that ceramic coatings are extensively microcracked during deposition. It is presumed that the density and distribution of these cracks plays a large role in the mechanical properties of the coatings.

Acoustic Emission Observations

Acoustic emission techniques have been coupled with tensile adhesion tests and metallography to ascertain the failure mechanism(s) of plasma-sprayed coatings. Consider a YSZ powder that was plasma-spray quenched into water to examine the degree of particle melting (Fig. 40.6). These particles do not completely melt, which, when considered with the original powder shape, results in many sites for "keying" in other particles and also for crack nucleation.

Different AE spectra were generated during tensile adhesion tests of such coatings. The AE spectrum of the raw data displayed the count rate as a function of time. It is then possible to sort the count rate values in ascending order and to classify them in count rate intervals of 2×10^2 counts/sec. The "average time" for any specific count rate interval was calculated, and these values are graphed in Fig. 40.7 for three different tensile tests. For example, specimen 2 exhibited 3 time intervals (at 4, 6, and 8 sec) of between 1000 and 1200 counts/sec, so the average time for a count of 1100/sec is 6 sec.

There are obvious differences between these distributions. In one case (specimen 2), the count rate gradually increased during specimen loading, and this was typical of a monomodal distribution. The other tests (specimens 1 and 3) showed a decrease in count rate during loading, and this was representative of bimodal distributions centered about low and high count rates. The bimodal behavior can be rationalized in terms of cracking mechanisms. For example, the unmelted regions of the coating provide crevices



Figure 40.6 Plasma-spray quenched 8 wt. % Y₂O₃-ZrO₂ powder. Note the intricate topology and partial melting of some particles.

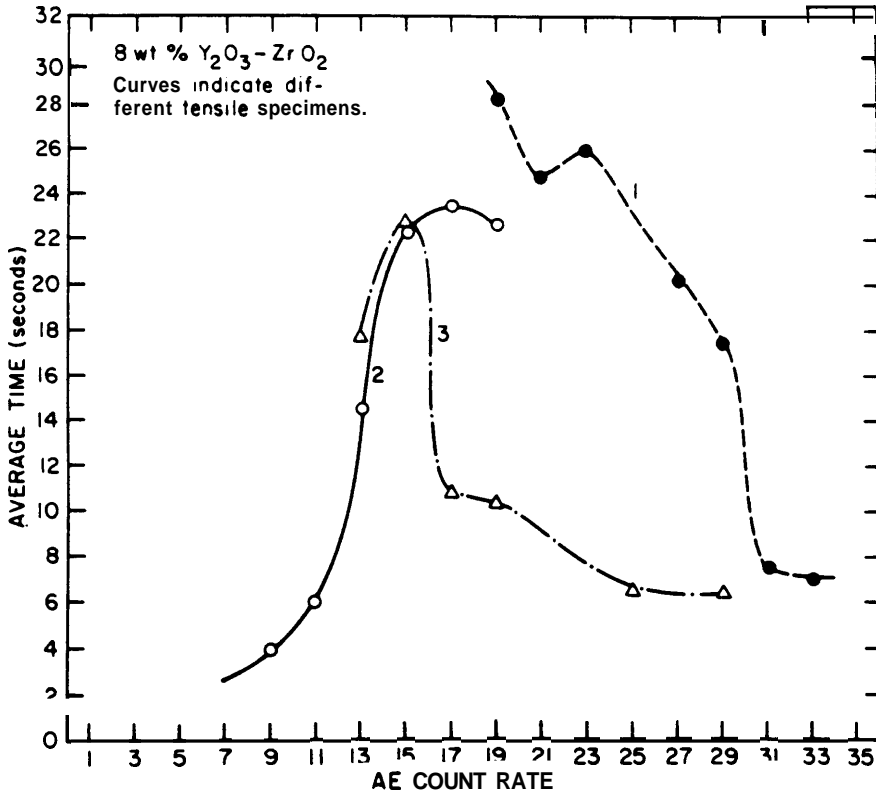


Figure 40.7 Summary of AE data derived from adhesion tests.

into which other semimolten particles flow. The net result is that the particles are integrally interlocked in many regions throughout the coating cross section. Acoustic emission phenomena arose from deformation and cracking about these regions during the initial (≈ 10 sec) straining of the sample and this gave rise to a high count rate. Subsequent cracking centered about the large microstructural features of the lamellae, with a corresponding decrease in AE. Specimen 3 was not as strong (34 MPa)* as specimen 1 (40 MPa), and this **difference** is reflected in a decrease in microcracking and AE activity.

However, it is now apparent that the monomodal distribution of specimen 2 disagrees with this fracture model. Failure in this case occurred in a mixed mode manner—that is, the coating failed at the substrate interface (adhesive), through the coating thickness (shear), and at the support layer interface (adhesive). Adhesion of the epoxy to the support bar was poor and it may not be appropriate to compare the AE spectra. The imperfect specimen preparation has, therefore, changed the stress distribution in such a manner that initial preloading does not generate AE events. It can be seen that AE analysis allows discrimination of failure mechanisms in plasma-sprayed coatings and that this phenomenon is related to the coating integrity and adhesion strength.

* Specimen 2 had a tensile strength of 36 MPa.

CONCLUSIONS

Plasma-sprayed coatings exhibit extremely complex microstructures with regard to their phase structure and lamellar interaction. The phase structure was characterized by metallographic techniques and a variety of microstructures were observed.

The adhesion of coatings was investigated via fracture toughness and tensile tests. Acoustic emission is valuable in formulating possible fracture mechanisms for YSZ coatings. In this case, it was thought that the semi-molten particles were a nucleus for cross-linking lamellae, and this improved coating integrity.

ACKNOWLEDGMENTS

This research originated under the auspices of the Australian Welding Research Association and has continued under those of the NASA Lewis Research Center. The author sincerely appreciates discussions with Reg McPherson, Ravi Shankar, and Herb Herman.

REFERENCES

1. I. A. Fisher, "Variables Influencing the Characteristics of Plasma-Sprayed Coatings," *Int. Met. Rev.* **17**, 117-129 (1972).
2. B. J. Scott and J. K. Cannell, "Arc-Plasma Spraying—An Analysis," *Int. J. Mach.* **7**, 243-256 (1967).
3. M. Nachman and A. Gheorghiu, "Melting of Particles Injected into a Plasma Jet," *Rev. Roum. Phys. (Rumania)*, **14**, 327-336 (1969).
4. A. Vardelle, M. Vardelle, and P. Fauchais, "Influence of Velocity and Surface Temperature of Alumina Particles on the Properties of Plasma Sprayed Coatings," *Plasma Chem. Plasma Process.* **2**, 255-292 (1982).
5. S. Safai and H. Herman, in *Treatise on Materials Science and Technology*, Vol. 20, H. Herman, Ed., Academic Press, New York, 1981.
6. D. A. Gerdeman and N. L. Hecht, *Arc Plasma Technology in Materials Science*, Springer-Verlag, New York, 1972.
7. B. Gross, B. Grycz, and K. Miklossy, *Plasma Technology*, Iliffe Books, London, 1968.
8. *Proceedings of The Seventh International Metal Spraying Conference*, The Welding Institute, Cambridge, 1974.
9. *Proceedings of The Eighth International Thermal Spraying Conference*, The American Welding Society, 1976.
10. *Proceedings of The Ninth International Spraying Conference*, Nederlands Instituut voor Lastechniek, 1980.

11. *Program of The Tenth International Thermal Spraying Conference*, to be published by the German Welding Society.
12. R. McPherson and B. V. Shafer, "Interlamellar Contact within Plasma-Sprayed Coatings," *Thin Sol. Films* **97**, 201–204 (1982).
13. V. Wilms. "Microstructure of Plasma Sprayed Ceramic Coatings," **Ph.D.** thesis, The State University of New York at Stony Brook (1978). Available from University Microfilms International, Catalog Number 7819123.
14. C. C. Berndt and R. McPherson, in *Materials Science Research Series*, Vol. 14, J. Pask and A. Evans, Eds., Plenum Press, New York, 1981.